DOI: 10.1002/ejoc.200700302

Structure of the Iron-Binding Exopolysaccharide Produced Anaerobically by the Gram-Negative Bacterium *Klebsiella oxytoca* BAS-10

Serena Leone,[a] Cristina De Castro,*[a] Michelangelo Parrilli,[a] Franco Baldi,[b] and Rosa Lanzetta[a]

Dedicated to Professor Matteo Adinolfi on the occasion of his 70th birthday

Keywords: Iron complexation / Exopolysaccharide / *Klebsiella oxytoca* / NMR spectroscopy

Klebsiella oxytoca BAS-10 is a Gram-negative micro-organism capable of growing on high concentrations of heavy metals. This bacterium produces large amounts of an iron-binding exopolysaccharide that, in the presence of metallic cations, precipitates as a dense gel. The primary and secondary structure of the repeating unit of such polysaccharide has been characterised by chemical and spectroscopic methods, resulting in the following heptasaccharide: 2)-α-Rha-(1→3)-β-Gal-(1→2)-α-Rha-(1→4)-β-GlcA-[β-GlcA-(1→4)]-(1→3)-α-Rha-(1→3)-α-Rha-(1→. The absolute configurations for the Rha units are L, while those for the GlcA and Gal residues are D.

Introduction

Bacteria of the *Klebsiella* genus are in general opportunistic pathogens responsible for nosocomial infection that can lead to severe diseases such as septicaemia, pneumonia, urinary tract infections and others.[1] In this genus there are a few distinctive species – *K. pneumoniae*, *K. oxytoca*, *K. planticola*, *K. ornithinolytica* and *K. terrigena* – though it is difficult to distinguish them by phenotypic testing.[2] Among *Klebsiella* strains isolated from hospitalised patients, *K. oxytoca* is the second most frequently encountered species. However, this species is also known as a nitrogen-fixing organism, and in the past a strain was isolated from rice rhizosphere.[3] Strains of *K. oxytoca* are known to produce exopolysaccharides of environmental[4] and pharmaceutical interest.[5]

A number of bacterial polysaccharides, produced either by Gram-positive or by Gram-negative bacteria, exhibit the ability to generate stable interactions with metallic cations. These complexes may form because of the electrostatic attraction between the positively charged ions and the negative charges of bacterial biopolymers. In fact, peptidoglycan, capsular or exocellular polysaccharides (EPSs), teichoic acids and lipopolysaccharides often provide efficient sites for the chelation of metals, due to the presence of acidic monosaccharides (such as uronic acids), phosphoryl or sulfonyl moieties and the carboxylic acid groups of some amino acids.[6] In addition, further chelation with the carbohydrate hydroxy groups supports the formation of the complex. Due to this great potential, it is possible to imagine the employment of these bacterial biopolymers in different fields. In bioremediation activity, heavy metals and radionuclides are among the major pollutants of soils and water, and their selective removal from the environment might be successfully achievable by means of these bacterial products.[7] Several bacterial polysaccharides have therefore been examined, and examples of polymers that can selectively bind different kind of metals at various amounts have been found.[1] Among these, a few examples of polysaccharides that specifically bind to Fe^{3+} have been discovered, including the capsular polysaccharide from *Bacillus licheniformis*[2] and the acidic exopolysaccharide from *Bradyrhizobium japonicum*.[3]

In this context, *K. oxytoca* BAS-10, isolated from iron-rich sediments (Tuscany, Italy) and classified on the basis of its 16S RNA sequence, is important, as this strain ferments ferric citrate to acetic acid and CO_2 and simultaneously produces conspicuous amounts of ferric hydrogel. This polymeric substance was preliminarily characterised by scanning confocal laser microscopy with the aid of the lectin Con-A conjugated with fluorescein to demonstrate the general polysaccharide composition of the ferric gel.[4]

[a] Department of Organic Chemistry and Biochemistry, University of Naples, Complesso Universitario Monte Sant' Angelo, Via Cintia 4, 80126 Napoli, Italy
Fax: +39081674393
E-mail: decastro@unina.it
[b] Department Environmental Sciences, Cà Foscari University, Calle Larga S. Marta, Dorsoduro 2137, 30123 Venice, Italy
Supporting information for this article is available on the WWW under http://www.eurjoc.org/ or from the author.

In this paper, the detailed chemical structure of this exopolysaccharide has been solved and its conformational properties are discussed.

Results and Discussion

Isolation and Purification of the Exopolysaccharide

After the anaerobic culturing of *Klebsiella oxytoca* BAS-10 in the presence of ferric citrate as carbon source, the formation of a dense iron gel at the bottoms of the culture flasks was observed. The iron gel, consisting of the exopolysaccharide complexed by Fe^{3+} together with *Klebsiella oxytoca* BAS-10 cells, was recovered from the culture medium by centrifugation. The pellet was then treated with a hot solution of EDTA in order to disrupt the interactions with the metallic cations and to permit the solubilisation of the polysaccharide material, allowing the removal of the cells by centrifugation. In order to remove the excess of EDTA, the supernatant was first dialysed against a solution of $CaCl_2$ and subsequently against water and then lyophilised. The obtained sample consisted of the EPS, still containing traces of iron cations, as evidenced by the ^{1}H NMR spectrum, in which the broad appearance of the peaks could be ascribed to the magnetic interference of the Fe^{3+} ions (Figure 1, a). In order to remove this complexed metal and to allow the characterisation of the polysaccharide, the sample was subjected to various purification steps. Initially, the sample was treated by gel permeation chromatography on a Sephacryl S-500 column, and two fractions containing the partially purified polysaccharide were collected. In particular, larger amounts of iron were present in the fraction eluted in the void volume, whereas the more strongly retained fraction showed a lower metal content, as is also visible from the appearance of the ^{1}H NMR spectrum (Figure 1, b), in which more finely resolved signals were now visible. This latter fraction was further purified by ion-exchange chromatography on a Q-Sepharose resin with elution with a linear NaCl gradient. The fractions obtained were desalted on a Sephadex G-10 column and freeze-dried. The most strongly retained fraction consisted of the pure exopolysaccharide. Its iron content was tested by atomic absorption spectroscopy and was found to be less than 0.01%, as confirmed by the enhanced resolution of the ^{1}H NMR spectrum of this sample (Figure 1, c). With this fraction, detailed structure elucidation was then performed by chemical and spectroscopic methods.

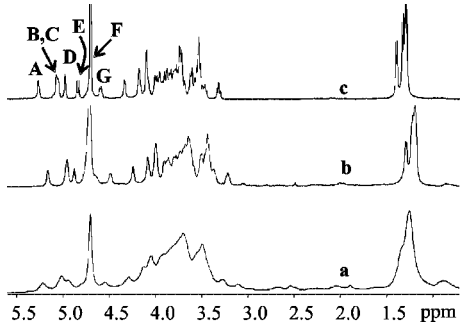

Figure 1. ^{1}H NMR spectra of the EPS from *Klebsiella oxytoca* BAS-10 after EDTA extraction (a), gel permeation chromatography (b) and anionic exchange chromatography purification (c). The increased sharpening of the signals is related to the progressive removal of the iron impurity from the sample. Spectra were recorded at 400 MHz and 305 K and the anomeric proton of **F** is covered by the residual water signal.

EPS Primary Structure Determination

Compositional analysis was performed as described[8] and revealed the presence of L-rhamnose (Rha), D-glucuronic acid (GlcA) and D-galactose (Gal) in a relative ratio of 4:2:1. Methylation analysis for detection of the glycosylation sites revealed the occurrence of 2-substituted-Rha (2-Rha), 3-substituted-Rha (3-Rha), 3,4-disubstituted-Rha (3,4-Rha), terminal-GlcA (*t*-GlcA), 4-substituted-GlcA (4-GlcA) and 3-substituted-Gal (3-Gal) in a relative ratio of 2:1:1:1:1:1. Fatty acid analysis did not detect any lipid component.

The ^{1}H NMR spectrum of the iron-free polysaccharide showed its best resolution at alkaline pH and contained seven signals in the anomeric region, between 5.2 and 4.5 ppm (labelled as **A**–**G** in order of decreasing chemical shift; see Table 1). Moreover, at high field, between 1.2 and 1.3 ppm, the signals of four methyl groups were identified and each was assigned to the 6-deoxy position of a Rha unit. The full proton resonance attribution for the identified spin systems was made possible on the basis of the 2D NMR spectra, in particular DQF-COSY, TOCSY and NOESY. Subsequently, on the basis of the ^{1}H,^{13}C-HSQC (Figure 2) and ^{1}H,^{13}C-HMBC spectra, the complete chemical shift assignment for the carbon atoms was accomplished. Residues **A**–**D** were identified as α-*manno*-configured, on the bases of the typical proton and carbon chemical shift values for the anomeric positions, of the low $^3J_{1,2}$ and $^3J_{2,3}$ coupling constants and of the diagnostic carbon chemical shifts for C-5.[9] In addition, TOCSY corre-

Table 1. ^{1}H (600 MHz, D_2O, 293 K), and ^{13}C (150 MHz) NMR chemical shifts (the latter printed in bold) of the EPS from *Klebsiella oxytoca* BAS-10.

	1	2	3	4	5	6a,b
A	5.188	4.022	3.886	3.458	3.738	1.244
2-α-Rha	**100.3**	**78.0**	**69.7**	**71.9**	**69.1**	**16.5**
B	4.969	4.013	3.805	3.455	4.026	1.20
2-α-Rha	**99.5**	**79.0**	**69.8**	**71.9**	**68.6**	**16.2**
C	4.969	4.264	4.089	3.734	3.880	1.31
3,4-α-Rha	**101.9**	**69.6**	**80.6**	**78.2**	**67.5**	**16.9**
D	4.891	4.107	3.765	3.483	3.698	1.216
3-α-Rha	**101.9**	**69.7**	**78.1**	**71.1**	**69.2**	**16.4**
E	4.779	3.219	3.437	3.444	3.649	–
t-β-GlcA	**102.4**	**73.4**	**75.7**	**72.0**	**76.5**	–
F	4.657	3.371	3.504	3.511	3.699	–
4-β-GlcA	**103.3**	**73.6**	**74.4**	**78.9**	**75.9**	–
G	4.504	3.620	3.667	3.928	3.664	3.824–3.605
3-β-Gal	**104.0**	**71.1**	**78.8**	**68.6**	**75.7**	**61.1**

lations from 1-H stopped at 2-H but the complete pattern was instead visible starting from 2-H, so all the residues were recognised as α-Rha. Spin systems **A** and **B** were identified as 2-Rha units, as confirmed by the downfield shift of the *C*-2 resonance due to glycosylation (78.0 and 79.0 ppm, respectively). Spin system **C** was identified as the 3,4-disubstituted Rha, on the basis of the glycosylation shifts observed for *C*-3 and *C*-4, whereas residue **D** was recognised as 3-Rha, according to the chemical shift for *C*-3, at δ = 78.1 ppm, which suggested substitution at *O*-3.

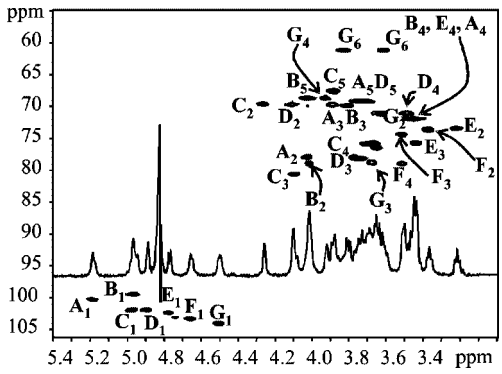

Figure 2. ^{1}H,^{13}C-HSQC spectrum and – overlaid – ^{1}H NMR spectrum (600 and 150 MHz, D_2O, 293 K) of the purified EPS from *Klebsiella oxytoca* BAS-10 recorded at alkaline pH. All the heteronuclear correlations are assigned and reported in Table 1; some densities are not labelled to avoid crowding in the spectrum.

Spin systems **E** and **F** were identified as two β-GlcA residues, on the bases of the large $^{3}J_{H,H}$ values and the typical appearance of the TOCSY spectrum, where the cross peaks for all ring positions were visible starting from the anomeric signal. The β-*gluco* configuration was further confirmed by the observation, in the 2D NOESY spectrum, of dipolar correlations between 1-H, 3-H and 5-H for both residues. In particular, spin system **E** was identified as the unsubstituted GlcA unit, whereas residue **F** presented a glycosylation shift corresponding to its *C*-4 (δ = 78.9 ppm) and was unambiguously recognised as the 4-GlcA unit.

Finally, residue **G** was identified as the 3-Gal residue (*C*-3 at δ = 78.8 ppm). Chemical shift values for the anomeric position revealed the occurrence of a β-configured residue, while the *galacto* configuration was deduced from the weak 3-H/4-H correlation in the DQF-COSY spectrum related to the small $^{3}J_{3,4}$ value (3 Hz). No 4-H/5-H correlation was visible at all, and the identification of the 5-H chemical shift was only made possible by the observation of a NOE correlation with 4-H, 3-H and 1-H protons in the NOESY spectrum.

The sequence of the heptasaccharide repeating unit was then inferred with the help of the NOESY (Figure 3) and HMBC spectra, in which interresidual dipolar or scalar correlations could be detected. In particular, in the anomeric region of the NOESY spectrum, the following diagnostic cross peaks could be detected: 1**A**-H/3**G**-H, 1**B**-H/4**F**-H, 1**C**-H/3**D**-H, 1**D**-H/2**A**-H, 1**E**-H/4**C**-H, 1**F**-H/3**C**-H and 1**G**-H/2**B**-H. All of these correlations were further confirmed by analysis of the long-range correlations evidenced in the HMBC spectrum and were in agreement with the previous methylation results. The primary structure of the repeating unit of the exopolysaccharide from *Klebsiella oxytoca* BAS-10 is thus summarised in Figure 4.

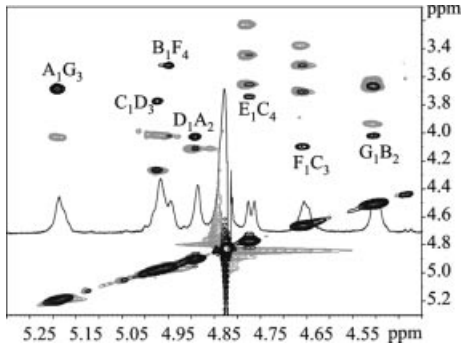

Figure 3. Zoom into the anomeric region of the TOCSY (grey) and NOESY (black) of the EPS from *Klebsiella oxytoca* BAS-10. Diagnostic interresidual correlations are indicated with capital letters referring to the spin systems described in Table 1.

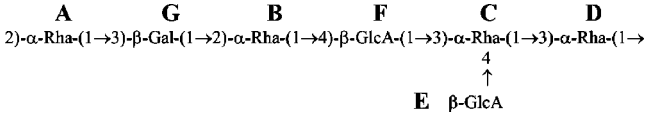

Figure 4. Repeating unit structure of exopolysaccharide isolated from *K. oxytoca* BAS-10; all rhamnose units possess the L absolute configuration whereas the other residues are D.

Conformational Analysis of Exopolysaccharide

In order to gain further information regarding the conformation of this polysaccharide, the following tetradecasaccharide was built:

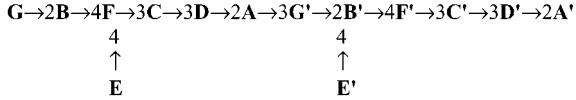

The letters reflect the NMR spectra labelling and this species represents two repeating units; interatomic distances and dihedral angles were extracted only for the inner residues whereas the units at the terminal edges (G and A′) were not considered.

In the preliminary part of the work, a grid search approach was used to find the optimal Φ, Ψ dihedral angles for each glycosidic junction; when more minima were present, the lowest in energy was selected (see Figure S1 – in the electronic supporting information – and Table 2) to build the complex oligosaccharide used in turn as the starting structure for the molecular dynamic calculations.

Table 2. Optimal dihedral angles determined for each glycosidic junction by a grid search approach. When more minima are present, they are listed in increasing order of energy and the lowest one is selected for the construction of the tetradecasaccharide used in the molecular dynamics simulation. Energies are in kJ mol^{-1}.

	Junction	Φ	Ψ	*E*
Gal-(1→2)-Rha	**G–B**	+61.1	–16.8	117.8
GlcA-(1→3)-Rha	**F–C**	+59.3	–28.6	106.9
GlcA-(1→4)-Rha	**E–C**	+56.4	+23.4	112.7
Rha-(1→2)-Rha	**D–A**	+54.8	+23.8	113.2
		+37.5	–48.6	113.4
		–34.5	–36.6	121.0
Rha-(1→3)-Gal	**A–G**	+59.3	+32.2	116.5
		–35.6	–38.0	125.6
Rha-(1→3)-Rha	**C–D**	+58.7	+30.7	118.7
		–35.8	–37.2	127.4
Rha-(1→4)-GlcA	**B–F**	+36.5	–48.0	108.6
		+65.7	+46.7	111.8
		–58.1	–55.2	119.0

Molecular dynamic simulation data were validated by simulation of the NOEs' effects for the overall ensemble of conformations (with the NOEPROM program) and comparison of the results with the experimental data (Table 3). In the course of this analysis, all the NOEs measured for the anomeric protons were confirmed and new correlations, previously unassigned, were identified and found to be consistent with the determined structure.

Table 3. Comparison of simulated and experimentally determined interproton distances for the tetradecasaccharides representative of two repeating units of the exopolysaccharide produced from *K. oxytoca* BAS-10.

Proton pair	Experimental distance	Simulated distance
$\mathbf{A_1G_3}$	_[a]	2.50[a]
$\mathbf{A_1G_2}$	2.78	3.38
$\mathbf{A_1G_4}$	3.89	4.28
$\mathbf{A_1D_5}$	_[a]	2.45[a]
$\mathbf{A_5G_4}$	2.94	2.49
$\mathbf{C_1D_2}$	3.44	3.79
$\mathbf{C_1D_3}$	2.50	2.44
$\mathbf{D_2C_5}$	2.20	2.46
$\mathbf{B_1F_4}$	2.26	2.33
$\mathbf{B_5F_3}$	3.29	2.78
$\mathbf{D_1A_2}$	2.21	2.40
$\mathbf{D_1A_3}$	3.40	3.99
$\mathbf{E_1C_4}$	2.56	2.62
$\mathbf{F_1C_2}$	3.55	3.42
$\mathbf{F_1C_3}$	2.37	2.41
$\mathbf{G_1B_2}$	_[b]	2.51

[a] A_1G_3 cross peak partially overlaps with that of A_1D_5; these two distances are not calculated. [b] For residue **G**, interproton distances are not calculated because all cross peaks necessary for the internal distance calibration are overlapped by other signals.

Analysis of the dynamics data was then extended and, in order to elucidate the flexible behaviour of the whole molecule, Φ and Ψ values were extracted (Table 4) and visualised both as scattered (Figure S2) and as time trajectories graphics (Figure S3). To interpret the data, Φ and Ψ values were assigned to three different groups on the bases of the root mean squared deviations (RMSDs) calculated on the whole ensemble of conformations: the first group (including elements with RMSD < 20) contained most of the Φs and some Ψs, with the other dihedral angles being included mainly in the second group (20 < RMSD < 30) and with only Ψ_B and $\Psi_{B'}$ belonging to the third group (RMSD > 30). This classification proved useful for handling of the extracted parameters and also allowed rational distinction between those junctions retained as flexible and those that were more rigid. Actually, linkages with either Φ or Ψ belonging to the third group display an elevated flexibility as in the case of **B** or **B′** junctions, while on the other hand, linkages with both Φ and Ψ inside group 1 are very rigid, as in the case of **E**, **A** and **E′** junctions and in agreement with visual inspection of the corresponding Φ/Ψ scattering plot (Figure S2); clearly, when either Φ or Ψ fall in group 2, the flexible behaviour of the glycosidic linkage is intermediate.

Table 4. Statistical data [averaged values and root mean square deviations (RMSDs)] of Φ and Ψ obtained from molecular dynamics simulation of the tetradecasacccharide; data are listed in three different group according to the RMSD criteria.

Group	Angle	Mean value	RMSD
Group 1	Φ_F	+59.2	15.8
	Φ_C	+51.4	13.1
	Φ_E	+58.4	11.4
	Ψ_E	+23.7	14.4
	Φ_D	+47.0	14.1
	Φ_A	+51.7	12.4
	Ψ_A	+27.8	17.8
	$\Phi_{G'}$	+58.7	13.0
	$\Phi_{F'}$	+60.3	14.2
	$\Phi_{C'}$	+50.8	15.4
	$\Phi_{E'}$	+58.0	11.6
	$\Psi_{E'}$	+23.2	14.2
	$\Phi_{D'}$	+47.6	13.0
Group 2	Φ_B	+32.3	21.5
	Ψ_F	–18.5	21.7
	Ψ_C	+20.6	21.5
	Ψ_D	+13.1	27.8
	$\Psi_{G'}$	+12.3	26.3
	$\Phi_{B'}$	+36.4	21.5
	$\Psi_{F'}$	–18.7	20.0
	$\Psi_{C'}$	+19.9	23.0
	$\Psi_{D'}$	+12.9	29.0
Group 3	Ψ_B	–27.6	35.2
	$\Psi_{B'}$	–13.5	37.5

These data led to the identification of two rather stiff moieties (Figure 5) in the molecule, the first composed of residues **F**, **C**, **E** and **D**, with a well defined cleft, and a second smaller one involving residues **A**, **G′** and **B′**, with the appearance of a rod. These two rigid moieties do not maintain the same relative orientation because of the presence of residues **B** and **D** (the RMSD of Ψ_D is rather borderline in the group classification), which are the source of the flexible behaviour of the molecule. The energies of four different conformers (Figure 5, Table 5) were then calculated with consideration of all the possible combinations of the two lowest-energy dihedral angles of the flexible glycosidic junctions (residues **D** and **B′**), those connecting the

rigid moieties of the simulated tetradecasaccharide. Surprisingly, the four different conformers possess comparable energies, suggesting that in solution they rapidly interconvert.

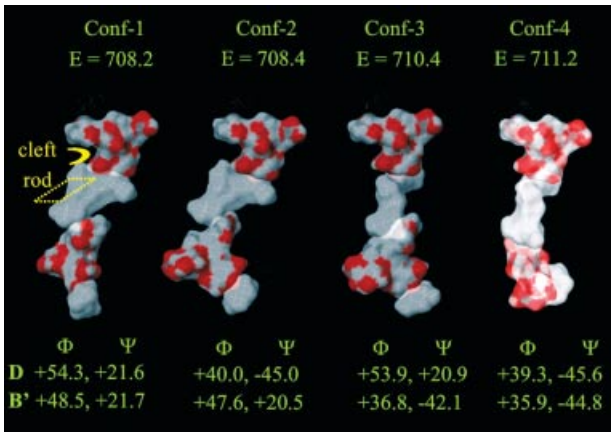

Figure 5. Representation of the four lowest-energy conformers of the simulated tetradecasaccharide. For each conformer, the Connelly surface was elaborated separately for the two rigid moieties; the more extended one forms a cleft and the oxygen atoms are coloured in red. The minor rigid moiety is depicted only in white and appears more rod-like in shape. The structural differences between the four conformers relate to the different relative orientations of the rigid segments.

Table 5. Dihedral angles and energies E (kJ mol^{-1}) of the four conformers calculated with consideration of all the possible combinations of the two lowest-energy dihedral angles of the flexible glycosidic junctions (residues **D** and **B′**).

	E	Φ_D	Ψ_D	$\Phi_{B'}$	$\Psi_{B'}$
Conf-1	708.2	+54.3	+21.6	+48.5	+21.7
Conf-2	708.4	+40.0	–45.0	+47.6	+20.5
Conf-3	710.4	+53.9	+20.9	+36.8	–42.1
Conf-4	711.2	+39.3	–45.6	+35.9	–44.8

This information poses two possibilities when considered in the light of the iron interaction topology: either the iron cation interacts with the fixed moiety of the molecule, or it interacts with one of the residues within the flexible domain of the molecule. In the first case, presumably the large cleft would be the potential binding site, being already preformed and ready to accommodate the metal; in the second case, the iron centre would need to shift the dynamic equilibrium to one of the conformers to reach the best accommodation, a feasible process, but with an associated energetic cost.

On the basis of the above considerations, the rigid moiety of the molecule, identified from the sequence **F**–(**E**)–**C**–**D**, was considered the best candidate for the Fe^{3+} ion coordination. Accordingly, the metal was tentatively docked (Figure 6) into this cavity, where some contacts (Table 6) in the 2.4–3.9 Å range with three residues – **C**, **F** and **D** – were detected. Unfortunately, it was not possible to derive more precise data. The problem was mainly associated with the lack of data related to the ferric ion properties of this sample. Actually, Fe^{3+} may exist either in high or in low spin state, and its coordination may vary accordingly (either penta- or hexacoordinate). The number of bonds with the sugar hydroxy functions would not necessarily be expected to fill the coordination sphere of the ion, since the solvent can be involved as well. In addition, the interaction with the hydroxy functions of the monosaccharide residues might involve hydrogen bond interactions with the solvent coordinated to the ferric ion.

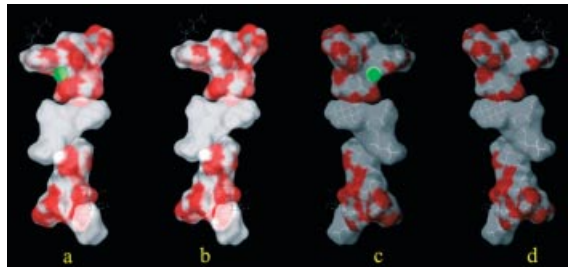

Figure 6. a) and c) Different views of the lowest-energy conformer with an iron atom (solid sphere) tentatively accommodated in the cleft. b) and d) As before, but without the metal.

Table 6. Interatomic distances for Fe^{3+} ion and lowest-energy conformation of the exopolysaccharide from *Klebsiella oxytoca* BAS-10.

Residue	Atom type and number	Distance
D	O_2	3.442
C	O_1	2.436
C	O_2	3.872
F	O_1	3.554
F	O_5	2.464
F	$O_{C=O}$[a]	3.104

[a] The distance reported is that with the closer oxygen on the carboxyl function, in this case the carbonylic one.

NMR Diffusion Measurements on the Exopolysaccharide

DOSY (Diffusion Ordered Spectroscopy) measurements were performed on the exopolysaccharide with increasing ferric ion concentration in order to gain additional information from the diffusion behaviour of the complex. The amount of $FeCl_3$ added to the polysaccharide was related to the number of repeating units of the exopolysaccharide, and samples with different stoichiometric ratios (0.1, 0.5 and 1.0) were analysed. The main effect found with increasing iron concentration was an equal broadening of all the proton NMR signals; although the addition was stepwise, we could not detect whether only some of the signals were modified preferentially with respect the others.

DOSY spectra were measured for each of these samples, but the mobility of the polysaccharide appeared to be unaffected (Figure S4).

Conclusions

Klebsiella oxytoca BAS-10, grown in anaerobic condition with Fe citrate as sole carbon source, produces an exopolys-

accharide with metal-chelating properties. The structure of this polymer is new (Figure 4) and consists of a heptasaccharide repeating unit.

The dynamic behaviour of this molecule was evaluated and it was possible to identify two rigid regions in the polysaccharide chain (Figure 5), one forming a cleft [residues **F**–(**E**)–**C**–**D**] and a second rod-shaped (**A**–**G**–**B**). The first motif appears to be a good candidate for the binding process, but more information should be acquired with further studies.

From a molecular point of view, this structure can be related to those of other polysaccharides from different *Klebsiella* species. For instance, the pentasaccharide repeating unit of the capsular polysaccharide from *Klebsiella* serotype K48[10] or the heptasaccharide from *Klebsiella* serotype K40[11] both contain rhamnose, galactose and glucuronic acid. In the present case, the relative orientation of the monosaccharides in the chain is different: probably the uronic acid moieties are implicated in the complexation with the metal ions and thus related to the peculiar sequestering ability showed by the polysaccharide.

Experimental Section

Bacterial Growth: Strain BAS 10 of *Klebsiella oxytoca* was grown anaerobically in a 5 L reactor. The medium contained (per litre): $NaHCO_3$ (2.5 g), NH_4Cl (1.5 g), NaH_2PO_4 (0.6 g), KCl (0.1 g) and, as carbon source, Fe citrate (10 g). The medium had previously been boiled for 5 min to remove O_2 and then cooled under N_2 flow. The reactor was sealed and autoclaved, and after cooling the cells were inoculated (3.1 ± 0.2 protein mL^{-1}) at a final pH 7.5.

Isolation and Purification of the Exopolysaccharide: After 6 d of incubation at 28 °C, 1 L of culture was centrifuged and the pellet consisting of the cells and the iron gel was collected (4 °C, 3000 g). This sample (6.7 g) was treated with EDTA (100 mM, 200 mL, pH 7) at 50 °C for 3 h, in order to solubilise the polysaccharide by disrupting the coordination with the iron cations. After centrifugation (4 °C, 3000 g), the precipitated was again treated with the EDTA solution. The supernatants were pooled and dialysed (12–14 kDa molecular weight cut-off), first against $CaCl_2$ and then against water, and freeze dried. The obtained polysaccharide fraction (62 mg) was first purified by GPC on a Sephacryl S-500 column (120×1.5 cm; Pharmacia) in NH_4HCO_3 buffer (50 mM). The most strongly retained fraction (30 mg) was further purified by anionic exchange chromatography on a Q-Sepharose (3×0.75 cm; Pharmacia) column with a NaCl gradient from 10 mM to 1 M. The eluate was monitored by testing the carbohydrate content by colorimetric phenol assay. The most abundant fraction was eluted with a NaCl solution (1 M), and was desalted by GPC on a Sephadex G-10 column (50×1.5 cm; Pharmacia), with monitoring with a Knauer differential refractometer. The sample obtained contained the pure EPS fraction. The iron content was found to be less than 0.01% by atomic absorption spectrometry.

Atomic Absorption Spectrometry: Iron solutions were analysed for total metal content by flame atomic absorption spectrometry (FAAS), using standard procedures.[12a,12b] A Varian SpectrAA 220 atomic absorption spectrometer fitted with a MK7 burner was used.

Samples were aspirated directly into an air/acetylene flame with no previous treatment. The total iron concentrations were determined either by the calibration curve method or by standard additions. In all cases no differences exceeding the experimental uncertainty were observed.

The instrument was set according to the following parameters: i) the sensitivity (defined as the metal concentration that produces the transmittance of 1% or an absorbance of approximately 0.0044), ii) the instrument detection limit (defined as the concentration that produces an absorption equivalent to twice the magnitude of the background fluctuation) as follows: wavelength 248.3 nm, slit width 0.2 nm, instrument detection limit 0.013 mg L^{-1}, sensitivity 0.08 mg L^{-1}. Background correction was accomplished with a deuterium arc lamp.

Analytical reagent grade chemicals were used throughout this study. Stock grade 1000 ppm metal solutions, certified for metal and impurities content, were from ROMIL Ltd, Cambridge and from Inorganic Ventures Inc., Lakewood.

Standards for iron analysis were prepared daily by appropriate dilution of the stock solution with hydrochloric acid (3.6%). All the glassware was treated twice with warm diluted (1:1) hydrochloric acid and then rinsed with distilled and deionised water and dried.

Ultrapure metal-free water from a Milli-Q Millipore apparatus was also employed.

Compositional and Methylation Analysis: Monosaccharide analysis was achieved by GLC analysis of their *O*-methyl glycoside derivatives[9] whereas the absolute configurations of the monosaccharides were assigned by GLC analysis of their 2-(+)-*O*-octyl glycoside derivatives by the described procedure.[13]

Methylation analysis was carried out as described.[14] For methylation analysis of the uronic acids, the exopolysaccharide was first carboxymethylated with methanolic HCl (0.1 M, 5 min), then methylated with diazomethane, and then reduced with $NaBD_4$ (4 °C, 18 h). The EPS was hydrolysed with trifluoroacetic acid (2 M, 100 °C, 1 h), reduced with $NaBD_4$, acetylated and analysed by GLC-MS.

GLC-MS was carried out on a Hewlett–Packard 5890 instrument with a SPB-5 capillary column (0.25 mm × 30 m, Supelco). For sugar methylation analysis and *O*-methyl glycosides derivatives the temperature program was: 150 °C for 2 min, then 2 °C min^{-1} to 200 °C for 0 min, then 10 °C min^{-1} to 260 °C for 11 min, then 8 °C min^{-1} to 300 °C for 20 min.

NMR Spectroscopy: NMR experiments were carried out on the exopolysaccharide at different stages of purification (Figure 1) with a Bruker DRX 400 MHz instrument fitted with a reverse multinuclear probe at 305 K.

For structural assignments of EPS, 1D and 2D ^1H NMR spectra were recorded with a solution of product (2 mg) in D_2O (0.6 mL) with NaOD (4 M, 5 μL). Experiments were carried out at 293 K on a Bruker DRX 600 fitted with a cryogenic probe. Spectra were calibrated with respect to internal acetone (δ_h = 2.225 ppm; δ_C = 31.45 ppm).

The NOESY experiment was measured with data sets of 1024×512 points, and 32 scans were acquired, with a mixing time of 200 ms employed. The double quantum-filtered phase-sensitive COSY experiment was performed with a 0.258 acquisition time with data sets of 4096×1024 points and 64 scans were acquired. The TOCSY experiment was performed with a spin-lock time of 120 ms and data sets of 1024×512 points; 16 scans were acquired. In all homonuclear experiments the data matrix was zero-filled in the F1 dimension to give a matrix of 4096×2048 points and was resolution-enhanced in both dimensions by a shifted sine-bell function before

Fourier transformation. The HSQC and HMBC experiments were measured using data sets of 2048 × 256 points, 64 scans were acquired for each t_1 value, and HMBC was optimised for a 6 Hz long-range coupling constant. In all the heteronuclear experiments the data matrix was extended to 2048 × 1024 points by forward linear prediction extrapolation.[15] All NMR analyses were carried out by literature procedures.[16]

2D DOSY spectra were acquired at 293 K with the Bruker sequence stebpgp1s using data sets of 32 K × 64 points, 8 scans were acquired for each increment, and the two key parameters Δ and δ (250 and 4.8 ms, respectively) were optimised on the 1D sequence. The sample (1 mg) was dissolved in deuterated phosphate buffer (15 mM, 400 μL) at pH = 7.0 in order to keep this last parameter stable during the increasing additions of ferric ions. $FeCl_3$ solution (0.092 M) was prepared in the same deuterated buffer solution, and consecutive additions of 1 μL (0.1 equiv. of Fe^{3+} with respect to the repeating units of the polysaccharide), 4 μL (in total 0.5 equiv. of Fe^{3+} ions with respect to the EPS repeating units) and 5 μL (in total 1.0 equiv. of ferric ions with respect to the EPS repeating units) were carried out. Following each addition, the sample was incubated overnight at room temperature to guarantee the establishment of the complexation equilibrium, and the measurement was carried out with insertion of a coaxial capillary into the NMR tube. The coaxial tube contained a solution of deuterated water and acetone (0.5 μL), used as reference for both chemical shift and diffusion measurements.

Molecular Mechanics and Dynamics Calculation: Molecular mechanics and dynamics calculations were performed using the MM3* force field as implemented in MacroModel 8.0, installed under the Red Hat Enterprise operating system. The MM3* force field used differs from the regular MM3 force field in the treatment of the electrostatic term, as it uses charge–charge instead of dipole–dipole interactions. The molecular mechanics approach was used to evaluate the optimal dihedral angles of all the glycosidic junctions of the repeating units; the calculations were performed with a dielectric constant ε = 80, as an approximation for the bulk water. Energy maps were calculated employing the DRIV utility (modulated with the DEBG option 150, which constrains the program to start each incremental minimisation reading the initial input structure file); in more detail, both Φ and Ψ were varied incrementally using a grid step of 18°, and each (Φ, Ψ) point of the map was optimised using 2000 P.R. conjugate gradients. Φ is defined as H_1–C_1–O–$C_{aglycon}$ and Ψ as C_1–O–$C_{aglycon}$–$H_{aglycon}$.

The plotting and the analysis of the relaxed surfaces was performed with the 2D-plot facility built into the MacroModel package; the flexible maps are shown in Figure S1. The oligosaccharide was built on the basis of the values at the minimum energy obtained and again minimised with the MM3* force field, but with approximation of the water solvent using the GB/SA model. Molecular dynamics simulation was started for each optimised structure, which was initially subjected to an equilibration time of 150 ps and successively kept in a thermal bath at 293 K for 4000 ps, a dynamic time step of 1.5 fs together with the SHAKE protocol to the hydrogen bonds was applied, coordinates were saved every 2 ps of simulation, leading to the collection of 2000 structures, and ensemble average distances between interresidue proton pairs were calculated from the dynamics simulation employing the NOEPROM program.[17] In particular, the spectra were simulated from the average distances r^{-6} calculated from the molecular dynamics simulation. Isotropic motion and a correlation time of 4000 ps were used to obtain the best match between experimentally determined and calculated NOEs for the intra-residue proton pairs.

Extraction of coordinates from molecular dynamics data was performed with the program SuperMap, supplied with the NOEPROM package, while graphic visualisation of Φ, Ψ glycosidic angles scattering was carried out with the Microsoft Excel™ program (Figures S2 and S3).

Elaboration of surface models was performed with the Surface utility of the MacroModel program and the Connelly model was chosen using the water probe radius of 1.4 Å; all atoms were white coloured with 50% of transparency and only in the extended rigid moiety are the oxygens red. The iron atom surface in Figure 6 is not transparent and is coloured green.

Supporting Information (see also the footnote on the first page of this article): Figures S1–S4.

Acknowledgments

The authors thank Prof. Carla Manfredi for help during the atomic absorption measurements and the "Centro di Metodologie Chimico-Fisiche" (CIMCF) of the University Federico II of Naples and Bioteknet for NMR facilities.
The authors declare no conflict of interests.

[1] F. Grimont, P. A. D. Grimont in *The Prokaryotes* (Ed.: A. Balows), Springer, New York, **1992**.
[2] G. Kotunovych, T. Lytvynenko, V. Negrutska, O. Lar, S. Brisse, N. Kozyrovska, *Res. Microbiol.* **2003**, *154*, 587–592.
[3] Y. Hirota, T. Fujii, Y. Sano, S. Iyana, *Nature* **1978**, *276*, 416–417.
[4] F. Baldi, A. Minacci, M. Pepi, A. Scozzafava, *FEMS Microbiol. Ecol.* **2001**, *36*, 169–174.
[5] R. Sugihara, M. Yoshimura, M. Mori, N. Kanayama, M. Hikida, H. Ohmori, *Immunopharmacology* **2000**, *49*, 325–333.
[6] D. L. Gutnick, H. Bach, *Appl. Microbiol. Biotechnol.* **2000**, *54*, 451–460.
[7] A. D'Annibale, V. Leonardi, F. Baldi, F. Zecchini, M. Petruccioli, *Appl. Microbiol. Biotechnol.* **2007**, *74*, 1135–1144.
[8] C. De Castro, O. De Castro, A. Molinaro, M. Parrilli, *Eur. J. Biochem.* **2002**, *269*, 2885–2888.
[9] G. M. Lipkind, A. S. Shashkov, Y. A. Knirel, E. V. Vinogradov, N. K. Kochetkov, *Carbohydr. Res.* **1988**, *175*, 59–75.
[10] J. P. Joseleau, M. F. Marais, *Carbohydr. Res.* **1988**, *179*, 321–326.
[11] A. K. Ray, A. Roy, N. Roy, *Carbohydr. Res.* **1987**, *165*, 77–86.
[12] a) G. F. Kirkbright, M. Sargent in *Comprehensive Analytical Chemistry* (Ed.: G. Svehla), vol. IV, Elsevier, Amsterdam, **1975**; b) *Official Methods of Analysis of the AOAC* (Ed.: W. Horwitz), 17th ed., Gaithersburg, **2000**.
[13] K. Leontein, J. Lönngren, *Methods Carbohydr. Chem.* **1978**, *62*, 359–362.
[14] I. Ciucanu, F. Kerek, *Carbohydr. Res.* **1984**, *131*, 209–217.
[15] J. C. Hoch, A. S. Stern, in *NMR Data Processing* (Eds.: J. C. Hoch, A. S. Stern), Wiley Inc., New York, **1996**, 77–101.
[16] T. Weimar, D. R. Bundle, in, *NMR Spectroscopy of Glycoconjugates* (Eds.: J. Jimenez-Barbero, T. Peters), Wiley-VCH, Weinheim, **2003**, pp. 109–144.
[17] J. L. Asensio, J. Jiménez-Barbero, *Biopolymers* **1995**, *35*, 55–75.

Received: April 4, 2007
Published Online: August 20, 2007

